scientific reports

OPEN

Highly compact dual-band frequency selective surface for path-loss and coverage improvement in millimeter-wave advanced wireless applications

Shahid Khan[1], Bilal Tariq Malik[1] & Slawomir Koziel[1,2✉]

In this work, a compact dual-band frequency selective surface (FSS) for path-loss and coverage improvement in advanced wireless communication is showcased. The proposed FSS is a single-layer design with stable and high performance at both 24 GHz and 38 GHz operating frequencies, respectively. The design is highly compact with two wide-band reflection coefficient responses having 49.5% (14.5–26.4 GHz) and 66.57% (35.8–39.8 GHz) bandwidth respectively. To the best of the author's knowledge, the proposed structure is the most compact design reported thus far with $0.14\lambda_0 \times 0.14\lambda_0$ electrical length at the lower cutoff frequency. With the proposed design architecture, it is easy to reconfigure the FSS. The small size of $2.95 \times 2.95 \, \mathrm{mm}^2$ enables effective operation in different communication environments. For coverage improvement and experimental validation, a 32×32 element array of the total footprint of $96 \times 96 \, \mathrm{mm}^2$ is fabricated and measured. The measured results demonstrate a significant coverage enhancement of up to 35 dB, for the Ku band, N257, and N260 millimeter wave (mm-wave) 5G bands. The proposed design is useful to enhance 5G mm-wave communication by tackling the fading effects or the presence of obstacles.

The recent advancements in the 5G wireless communication domain have necessitated the design of compact and high-performance wireless devices. Due to high frequency, 5G mm-wave wireless devices' operation is impacted by changing geographical terrains, rainy weather, and obstacles in the form of high-rise buildings. To address these challenging issues, 5G devices must be equipped with small-size and high-quality front ends[1]. Performance enhancement is possible either by designing a better antenna or by adding an external layer in the form of frequency selective surface (FSS), reflective intelligent surface (RIS), or electromagnetic band gap (EBG) structures[2]. Numerous techniques for performance enhancement have been proposed in the literature. These include MIMO arrangements, array configurations, and the addition of an EBG surface to the antenna design, all bringing limited improvements while increasing the design complexity[2,3]. Among these techniques, adding a metamaterial surface to the transmitting and receiving ends may considerably improve the coverage and overall functionality.

Numerous frequency bands, which include n257 (26.5–29.5 GHz), n258 (24.25–27.5 GHz), n259(39.5–43.5 GHz), n260 (37.0–40.0 GHz), and n261 (27.50–28.35 GHz) are specified for 5G and beyond communications[2]. These operating bands are associated with wideband, high data rates, and low latency. However, due to the shorter wavelength, the mm-wave communication is impacted by obstacles that deteriorate line of sight (LOS) communication. Deploying advanced wireless networks including 5G and beyond in interior spaces with high user densities, such as conference rooms, stadiums, airports, walls, and other significant impediments can readily block millimeter-wave transmissions[4]. In non-line-of-sight communications, this may result in coverage deterioration and link instability. RIS and FSS act as intelligent mirrors and offer an alternative way to enhance the coverage by improving the gain[5]. As seen in Fig. 1, they enable the establishment of an alternative channel for the signal, allowing for a stable connection even in the presence of certain impediments. In 5G mm-wave

[1]Faculty of Electronics, Telecommunications, and Informatics, Gdansk University of Technology, 80-233 Gdansk, Poland. [2]Engineering Optimization and Modeling Center, Reykjavik University, 101 Reykjavik, Iceland. ✉email: koziel@ru.is
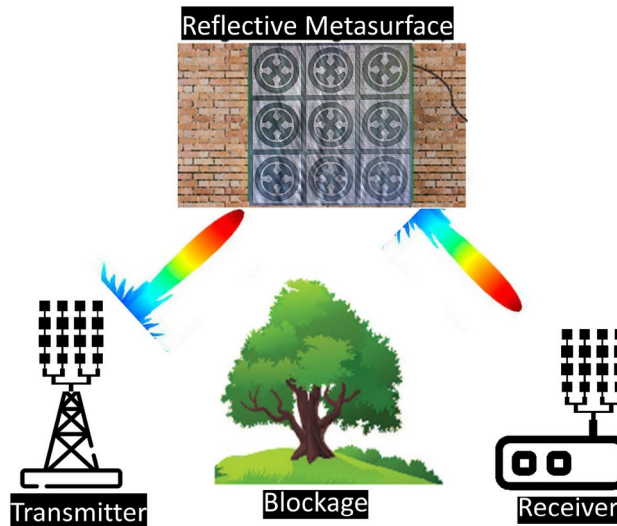
Fig. 1. Overview of the FSS design architecture and working principle.

communications, RIS is a potentially beneficial technique to enhance performance[2,6–10]. As RIS is becoming increasingly common for mm-wave frequency bands, a substantial amount of theoretical work on RIS to boost coverage has been published in the literature recently[5,8,9,11,12].

A thorough theoretical analysis demonstrating the application of RIS in wireless communication systems for coverage augmentation can be found in[11]. In[12], detailed theory and design aspects of the FSS are presented. The work encompasses all the basics and diverse FSS design procedures. Most published literature on FSS is based on sub-6 GHz frequencies[3,13], and only a handful of reports are available for mm-wave frequency bands for coverage improvement. In[14], a second-order polarization rotating FSS is discussed. The design has the potential of adopting polarization rotation however the drawback of the design is multiple layers and narrow fractional bandwidth. In[15], a band-pass FSS with a tiny periodic element is introduced, implemented on a single-layer substrate with a relative permittivity of 2.65. The unit-cell dimensions of this FSS are $0.058\lambda_0 \times 0.058\lambda_0$, ($\lambda_0$ representing the free-space wavelength corresponding to the resonant frequency) exhibits potential miniaturization capabilities. Although the design offers good performance, the drawback is the provision of performance on a single band, which limits its usefulness in real-world applications. Wu et al.[16] describes the development of an ultrathin frequency selective surface using a square unit cell containing three ring slot pairs loaded into it. There are metal shorts in the outer ring slot pair. One polarization-insensitive passband with a strong transition at the Ka-band is realized. While maintaining good performance, the design has a relatively large electrical length at the lowest cutoff frequency. In[17], a dual pass band FSS surface at 28.1 GHz and 39.5 GHz for 5G application is presented. The design features an overall electrical length of s $0.56\lambda_0 \times 0.56\lambda_0$. Although the design has shown promising results, the multi-layer structure and large unit cell dimensions are detrimental to its usefulness.

In contrast to the published literature, the proposed study is the first of its kind that offers FSS with two reflections and one transmission band while maintaining ultra-compactness. It demonstrates how, in non-line-of-sight communications, FSS can reduce the mm-wave path loss from transmitter to reciever. This boosts the signal strength up to 30 dB at all 5G mm-wave frequency bands and provides tangible evidence of coverage enhancement. The unique, ultra-compact, low-profile unit-cell design with a single-layer geometry is the foundation for the proposed FSS. The unit cell design achieves a high grazing angle of incidence stability up to $60°$, polarization-insensitive dual-band reflection compliance at 22 GHz and 38 GHz, and single-band transmission at 33 GHz. The original contribution and novelty of the proposed work are detailed as follows:

1. Design and execution of a single-layer FSS unit cell architecture to preserve small dimensions and low profile for mm-wave applications.
2. The proposed FSS unit cell design is polarization insensitive and has a stable transmission and reflection response for different angles of incidence up to $60°$.
3. The coverage enhancement measurements at all 5G mm-wave bands show up to 35 dB improvements in non-LOS path loss.
4. To the author's knowledge, this is the first compact FSS unit cell design with dual reflection and single transmission band as compared to the works reported in the literature.
5. It is a single-layer design, incorporating all the resonating structures in a single surface without additional layers, making our design compact, low cost, easy to manufacture, and integrate with other wireless devices.
6. The proposed design has the flexibility to return easily to other frequencies by readjusting the few design parameters as shown in Fig. 2.The rest of the paper is organized as follows. Section II elucidates the suggested FSS unit cell design, geometry evolution, and parametric analysis. The suggested FSS's implementation, measurements, and experimental validation of coverage augmentation are covered in detail in Section III. Section IV concludes the work.
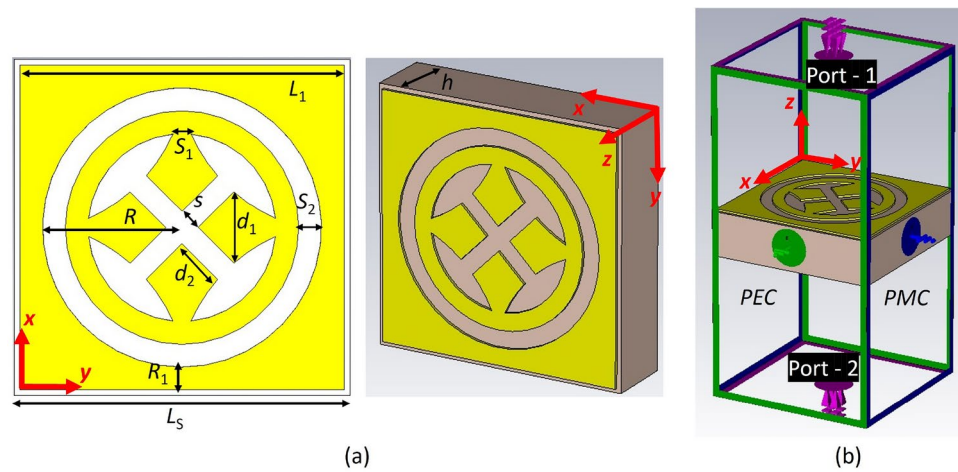
Fig. 2. Proposed unit cell: (**a**) front and side view, (**b**) simulation model of the FSS unit cell.

Proposed FSS design overview

The proposed reflective FSS comprises a large number of periodic passive unit cells arranged in a two-dimensional layout at regular intervals. These resonant structures can efficiently reorient incident electromagnetic waves in the appropriate direction. Passive FSS devices do not actively augment the incident wave's intensity in contrast to antenna arrays. By design, they modify the amplitude and phase of incident signals to either boost or reduce the signal strength. To increase 5G coverage, intelligent surfaces can be mounted on exterior trees, buildings, and walls. Low-profile, compact multiband FSSs exhibiting angular stability and polarization insensitivity are highly demanded for the mentioned applications. The following subsections provide an overview of the proposed FSS unit cell's geometry. The design evolution and parametric analysis are presented, and a comprehensive stability evaluation based on polarization and angle of incidence is conducted.

FSS unit-cell design

This section details the evolution of the design of the FSS unit cell. Figure 2a shows the geometrical configuration of the suggested FSS cell front and perspective views. The dielectric substrate employed in this study is 0.76 mm-thick Arlon AD 250 with a dielectric constant of 2.5 and a loss tangent of 0.0013. The proposed FSS unit-cell design is placed on the upper side of the dielectric substrate, whereas the bottom side has no copper layer. Figure 2a also details all the relevant dimensions of the unit cell. L_1 is the total length of the patch, S_1 is the thickness of the lower part of the inner stacked patch, S is the gap between stacked patches, and R is the radius of the inner ring. S_2 is the gap between the outer patch and the inner ring. R_1 is the thickness of the outer patch while d_1 and d_2 are the length and width of the diamond-shaped patch. h and L_s are the thickness and length of the substrate, respectively. The suggested FSS is designed and simulated using CST Microwave Studio. The direction of the incident wave is along the z-axis, and the single-cell periodic boundary conditions are maintained along the xy-plane, as shown in figure as shown in Fig. 2b.

Stepwise design evolution and analysis

The FSS unit cell geometry is finalized in three steps. These steps and the corresponding reflection and transmission coefficients are depicted in Fig. 3a and b respectively. The suggested FSS unit cell design consists of several structures, such as the outer square loop, circular loop, and diamond-shaped patches, to enhance the design flexibility and scalability over a wide frequency range. The circular slot in the square patch is responsible for the transmission coefficient response at 30 GHz. Four symmetrical slots in the circular patch shift the transmission coefficient to the lower frequency with a wider response. Four additional slots in the inner circular patch introduce another wide reflection band resonating at 38 GHz. As seen in Fig. 4a, the proposed FSS includes one transmission band from 29.5 to 31.2 GHz and two reflection bands from 15 to 28 GHz and 35–42 GHz, with fractional bandwidths of 49.5% and 66.57%, respectively which are desirable for satellite and 5G mm-wave applications.

To explain the working principle of the unit cell, the equivalent circuit is developed and simulated in Keysight ADS as depicted in Fig. 4c. The gaps between the inner and outer circles and the gap between the diamond shapes exhibit capacitive effects, whereas the microstrip patch has inductive effects as shown in Fig. 4b. The simulated results show that both simulation responses closely follow each other. As shown in Fig. 4a, ADS simulation presents a better response in terms of impedance matching as it considers the ideal simulating environment. A minor shift in the reflection coefficient is also noticed. The ADS calculations show that L_1 and L_2 have values of 0.24 nH and 0.18 nH whereas capacitors C_1 and C_1 are 0.226 pF and 0.1 pF, respectively. Therefore, the lower (f_1) and upper (f_2) resonant frequencies of the proposed FSS can be shifted through the proper tunning of C_1, L_1, C_2, and L_2 by using Eq. 1:

$$f_n = 1/(2\pi\sqrt{(L_nC_n)}), \quad n = 1, 2 \tag{1}$$
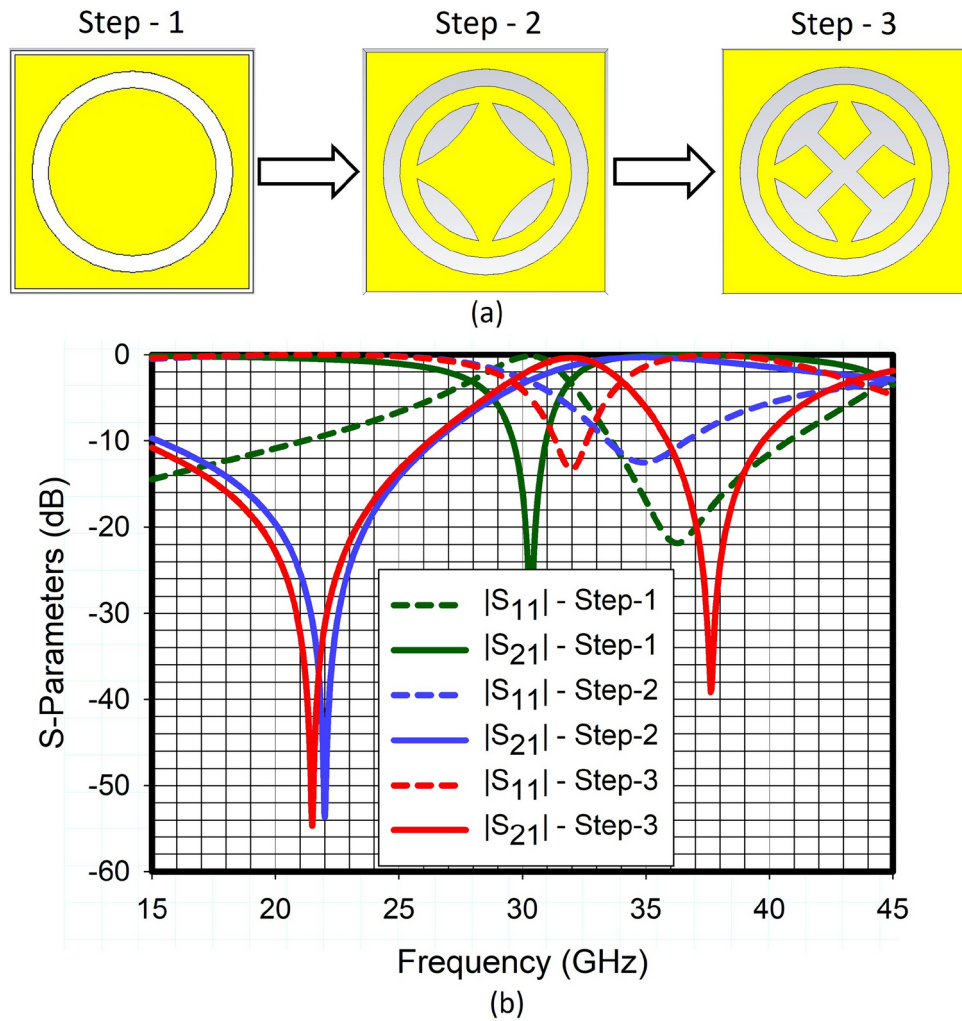
Fig. 3. Design steps of the proposed unit cell: (**a**) shape of the unit cell for each design step, (**b**) corresponding reflection and transmission coefficients.

Figure 4d shows the current distribution of the unit cell at 24 GHz and 38 GHz. The electric field is concentrated between the outer and inner circles, and less current activity is noticed on the inner patches. Thus, the gap between the inner and outer circles contributes to the lower frequency. At 38 GHz, the electric field is focused on the inner patches as shown in Fig. 4d. The higher frequency is influenced by changing the inner patch dimensions.

Parametric analysis

This section presents a thorough parametric study of the suggested FSS design. A comprehensive evaluation and optimization for all unit cell parameters has been performed via extensive full-wave simulations. These parameters include the dimensions of the outer patch L_1, the radius of the outer circular loop R, the gap between diamond-shaped patches S, the width of the lower part of the diamond-shaped patch S_1, the gap between the outer patch and the inner ring S_2, the thickness of the outer patch R_1, and the length and width of the diamond-shaped patches d_1 and d_2. These parameters impact the transmission and reflection performance of the proposed metasurface and are analyzed and discussed in detail. S_2 is the gap between the outer patch and the inner ring R. R_1 is the thickness of the outer patch whereas d_1 and d_2 are the length and width of the diamond-shaped patch. S_2 enhances the capacitive effect, which causes the S-parameter response to shift toward lower frequencies. In contrast, decreasing S_2 has the opposite effect, shifting the S-parameters to higher frequencies. Similarly, the parameters d_1 and d_2 of the diamond-shaped patch represent inductive effects. Any increase or decrease in these values will also cause corresponding shifts in the S-parameters, either towards higher or lower frequencies, depending on the implemented variations. The unit cell's outer circular loop controls the lower transmission band, while the diamond-shaped patches generate the upper band. The gap between the patches helps to control the resonant frequency of the upper band. To illustrate the above concept, Fig. 5 displays the results of parametric analysis of the geometric variables S, S_1, and R and the impact of the scaling factor.
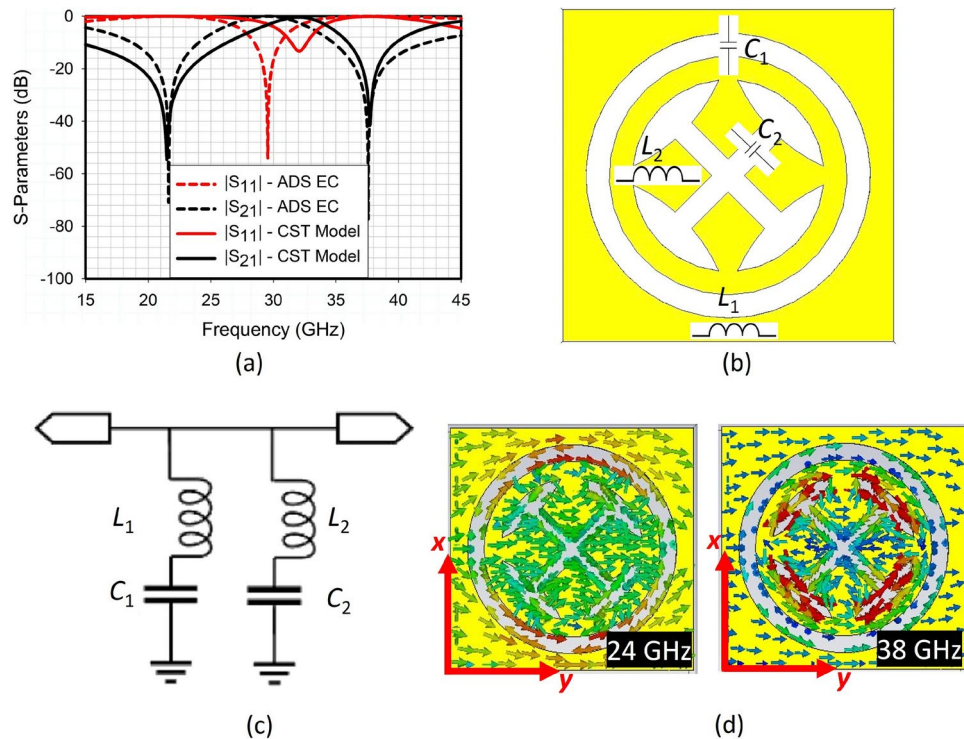
Fig. 4. (**a**) Reflection coefficients comparison obtained from CST and ADS, (**b**) capacitive and inductive effects from different parts of the unit cell, (**c**) equivalent circuit of the design unit cell, (**d**) surface current distribution.

Figure 5a details the impact of the gap between the diamond-shaped patches. Increasing the gap shifts the upper resonant frequency band to higher values. When the gap is enlarged from 0.2 to 0.3 mm, the upper band shifts from 38 to 40 GHz. However, the gap does not affect the lower band and the single transmission band. Figure 5b shows the impact of the patches lower part. It is evident that increasing the patch width only impacts the upper band, whereas the lower reflection and transmission band retain their position. Figure 5c shows the impact of the outer loop radius on the reflection and transmission band. Increasing the outer loop radius impacts the lower reflection while it does not visibly affect the upper reflection band and transmission band. Changing the value from 2.4 to 2.5 mm shifts the lower reflection band from 21.5 to 22 GHz. Figure 5d shows the impact of linear scaling up or down the overall dimensions of the unit cell on the reflection and transmission band. Reducing the overall dimensions shifts both the transmission and reflection bands to higher values, and increasing the overall dimensions shifts all operating bands toward the lower range. This validates the simple reconfigurability of the proposed FSS design. Table 1 summarizes the optimized values of the proposed FSS design.

Figure 6a and b shows the reflection and transmission response of the suggested FSS design evaluated using CST Microwave Studio for different polarization and incidence angles. It can be concluded that for both TE (transverse electric) and TM (transverse magnetic) orientations, the structure's symmetry results in relatively constant transmission and reflection coefficients when the angle of the incident of EM (electromagnetic) waves is changed within the range of $\pm 60^\circ$. To validate the proposed unit cell efficacy, an array consisting of 32×32 unit cells with a total surface size of $96 \times 96 \, \text{mm}^2$ was also designed and simulated. The simulated results of large FSS show the stable reflection and transmission response of the proposed design.

Experimental setup and measured results

This section details the reflectance/transmittance results obtained from the fabricated FSS prototype. This section also explains an experimental demonstration of the coverage enhancement for the 5G mm-wave bands. The developed design of the proposed metamaterial surface has been fabricated and verified under various scenarios following extensive numerical simulations. The proposed surface has a total dimension of $96 \times 96 \, \text{mm}^2$. It is arranged as an array of 32×32 unit cells. Figure 7c shows the fabricated prototype's front view and microscopic image. All measurements were carried out in the anechoic chamber. Figure 7a and b demonstrate the transmission and reflection coefficient measurement setup, respectively. As shown in Fig. 7a, the proposed FSS is placed between a transmitting and a receiving antenna at a distance d between the FSS and the horn antennas which are connected to the VNA. The transmitted signal through the FSS surface and in free space is recorded. In the case of S_{11} measurement, both horn antennas are positioned side by side in front of FSS, with S_{11} extracted by comparing the transmission response obtained with FSS and, subsequently, with the PEC board placed instead of the FSS. Figure 8a and b show the comparison between simulated and measured reflection
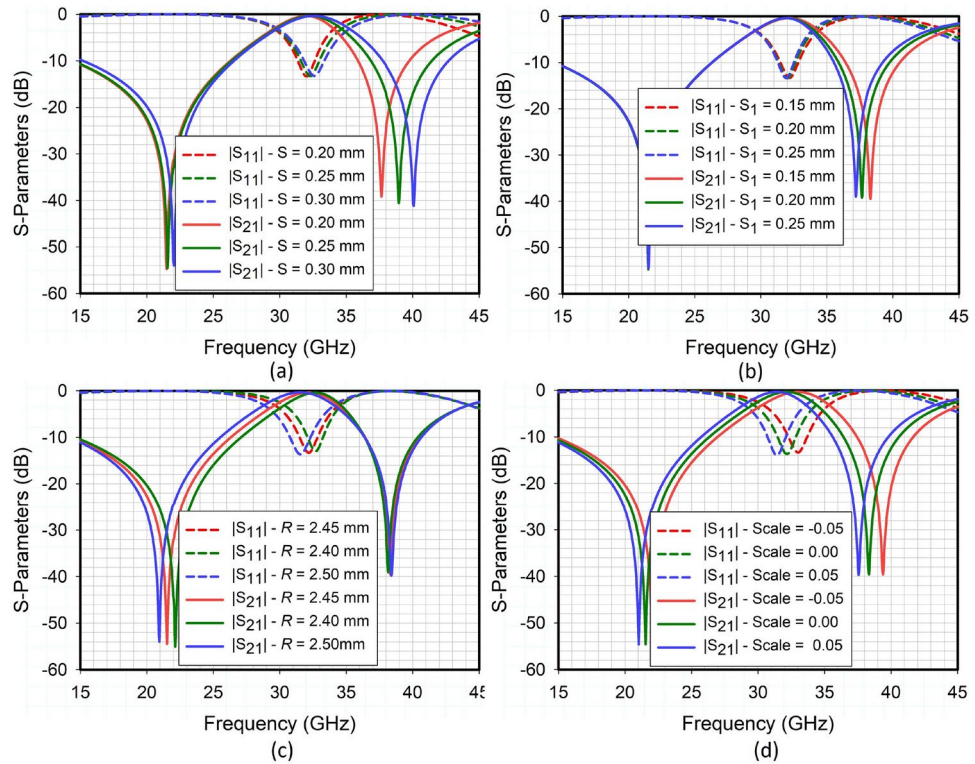
Fig. 5. Impact of different parameters on S-parameters response.

Parameters	Dimensions (mm)	Parameters	Dimensions (mm)
L_s	2.95	L_1	2.85
R	2.45	S_1	0.2
S	0.2	h	0.76
R_1	0.2	S_2	0.2
d_1	0.623	d_2	0.44

Table 1. Optimized design parameters of proposed FSS.
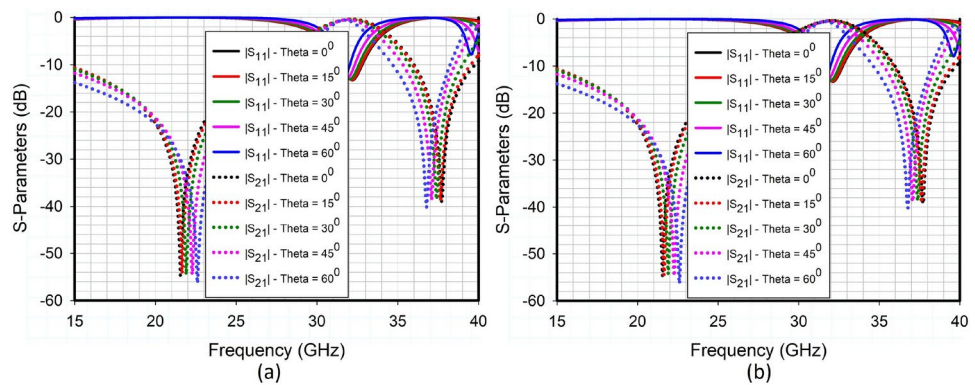
Fig. 6. Impact of varying incident angle on S-parameters: (**a**) TE polarization, (**b**) TM polarization.

and transmission response, respectively, of the proposed FSS. There is good agreement between the simulated and measured results. However, the major sources of deviations between the simulated and measured results are fabrication inaccuracies, positioning of the measurement setup components (horn antennas, measured FSS, and the PEC board), as well as frequency limitations of the reference antennas (especially below 18 GHz).
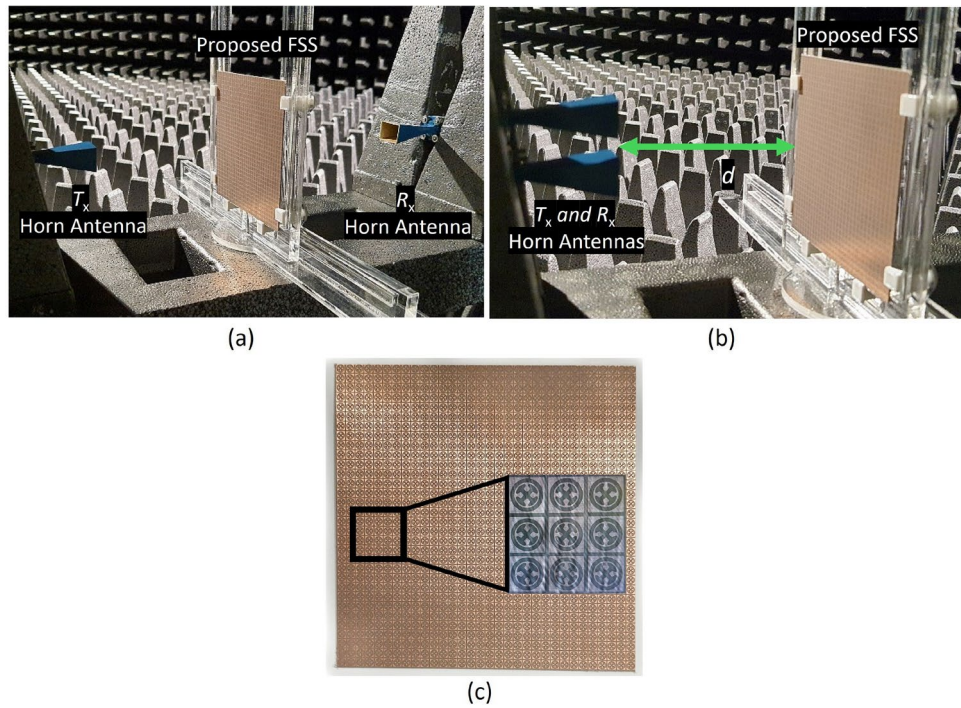
Fig. 7. Experimental setup for measuring (**a**) transmission coefficient, (**b**) reflection coefficient, and (**c**) fabricated prototype.
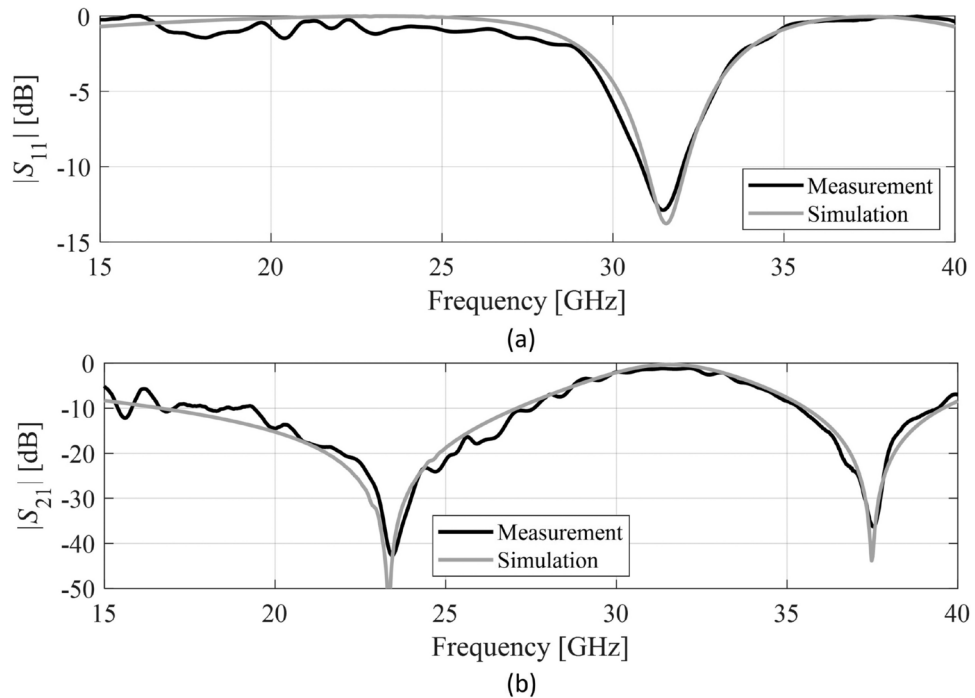

Fig. 8. Scattering parameters (**a**) simulated and measured reflection coefficient, (**b**) simulated and measured transmission coefficient.

Among these, the most important factor is positioning consistency. In particular, accurate allocation of the PEC board (in place of the FSS) when doing comparative transmission response measurements, both in terms of the distance and angle plays a crucial role in achieving reliable results. Other factors have less significant effects. The inter-element spacing can be further reduced by using more advanced etching technology. This would make the

design even more compact and allow us to incorporate a larger number of unit cells, thus providing enhanced coverage without increasing the FSS size.

Coverage enhancement measurements

This section explains the experimental demonstration of the coverage enhancement for mm-wave 5G applications. Figure 9a depicts the experimental setup for the coverage enhancement measurements. Two standard horn antennas are used in this measurement setup to transmit the incident waves on the FSS and then receive the reflected waves from the FSS. To impede the direct line-of-sight (LOS) path, an absorber or blockage is placed in between the transmit (T_x) and receive (R_x) antenna. To offer an additional transmission line and prevent obstruction the proposed FSS prototype is positioned parallel to (T_x) and (R_x), as shown in Fig. 9a. Figure 9b displays the measured transmission coefficient $(|S_{21}|)$ between the Tx and Rx. The received signal intensity at the (R_x) antenna is compared for three scenarios. In these experimental results, the first measured transmission response between the (T_x) and (R_x) corresponds to an absorber (without FSS), and the second one involves the signal received from the FSS. The third scenario incorporates a metallic sheet the same size as the FSS aperture. There is a discernible 23 dB enhancement (from -53 to -30 dB) in the operating band between 24 and 27 GHz, and 35 dB enhancement (from -68 to -33 dB) within the operating band from 36 to 40 GHz when the PEC is substituted with the proposed FSS. Notably, there is no signal improvement on the proposed FSS's 30 GHz transmission spectrum, which is the transmission band. Based on the experimental demonstration, the proposed FSS delivers a signal boost of 20–35 dB spanning the entire 5G bands and a portion of the Ku band. The results of these experiments validate that the proposed FSS design can enhance the mm-wave 5G communication for internet-of-things (IoT) and satellite communication devices.

Table 2 compares the proposed work with the state-of-the-art designs reported in the recent literature. In[2], a compact reflect array at 28 GHz is presented with a 20 dB signal enhancement. However, the design has no potential to address the polarization insensitivity problem. In[6], a single band reflectarray operating at 28 GHz is detailed. Although the design is compact and features polarization insensitivity, its drawback is its multi-layer structure. In[7], a two-layer structure array operating at two bands is presented for mm-wave 5G applications. In[18], a compact single layer single band reflect array is presented with an asymmetric design, which leads to polarization sensitivity and stability issues. In[19], a two-layer reflect array with a dual-band response is presented. The design achieved an incident angle stability of up to 45°. In[22], a compact reflect/transmit array for coverage enhancement of up to 25 dB is presented. Comparing the suggested unit cell geometry to the benchmark structures shown in Table 2, it is incredibly compact. With polarization insensitivity, the suggested FSS has incidence angle stability of up to 60° which is superior to most of the works reported in Table 2. Compared to
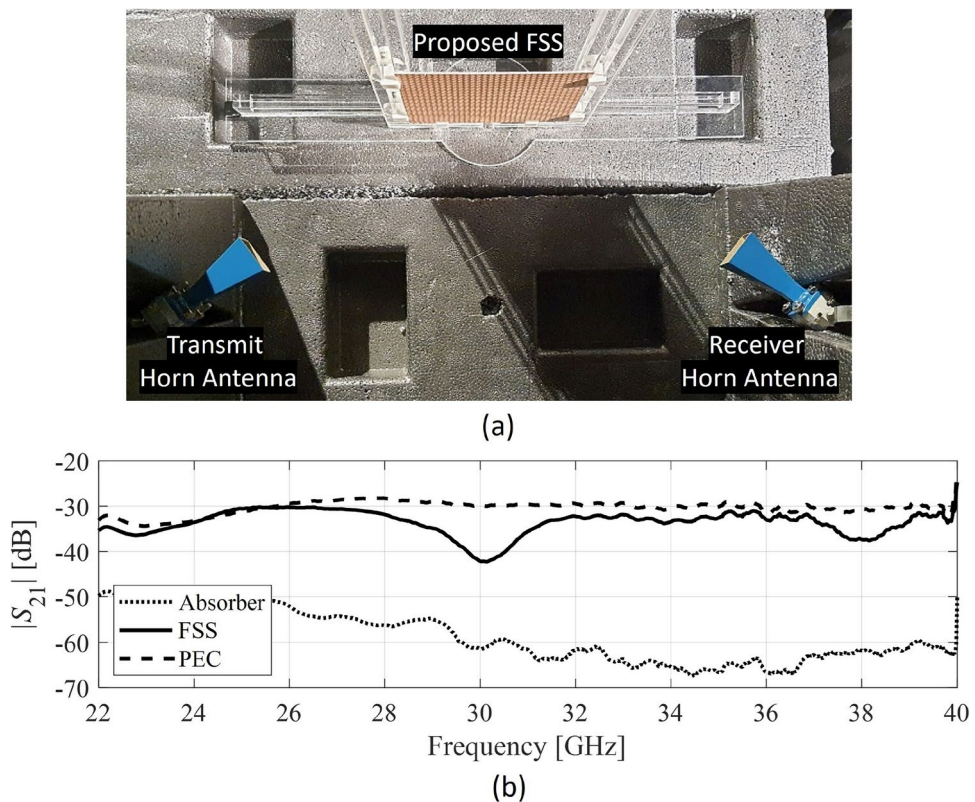

Fig. 9. Coverage enhancement, (**a**) experimental setup, (**b**) comparison of transmission response $(|S_{21}|)$ based on the absorber, PEC, and the proposed FSS.

Ref.	Layer	Substrate/thickness (mm)	Unit-cell type	Operating bands (GHz)	Polarization insensitivity	Bandwidth (GHz)	Unit-cell size (mm)	Pathloss improvement (dB)
[2]	Multi	Rogers/FR4	Reflective	28	No	22.7–30.5	$3.85 \times 3.85/0.29\lambda_0 \times 0.29\lambda_0$	15–20
[6]	Two	RT5880/0.79	Reflective	28	Yes	23.96–45.9	$3 \times 3/0.23\lambda_0 \times 0.23\lambda_0$	N/A
[7]	Two	RT5880/0.254	Reflective	28, 38	Yes	20–30.9, 35.28–45	$4 \times 4/0.26\lambda_0 \times 0.26\lambda_0$	N/A
[18]	Single	RT5880/0.79	Reflective	26	No	24.55–26.5	$5 \times 5/0.4\lambda_0 \times 0.4\lambda_0$	N/A
[19]	Multi	SCGA-500/0.76	Reflective	26, 38	No	16.03–39.09	$4.6 \times 4.6/0.25\lambda_0 \times 0.25\lambda_0$	N/A
[20]	Two	RO4003/0.51	Reflective	28	No	20–30	$4.2 \times 4.2/0.28\lambda_0 \times 0.35\lambda_0$	N/A
[21]	Two	RT5880/0.79	Reflective	24	No	24–28.8, 36.6–40.8	$2.7 \times 2.7/0.21\lambda_0 \times 0.21\lambda_0$	N/A
[22]	Single	AD250/0.76	Reflective/transmitive	24, 38, 30	Yes	19.5–26.2, 37.1–41.8	$3.3 \times 3.3/0.21\lambda_0 \times 0.21\lambda_0$	20–25
Proposed	Single	AD250/0.76	Reflective/transmitive	15, 24, 38, 30	Yes	14.5–26.4, 35.8–39.8	$2.95 \times 2.95/0.14\lambda_0 \times 0.14\lambda_0$	20–35

Table 2. Comparison of proposed research with related work in open literature.

the published literature, the proposed highly compact design has two reflective and one transmission band and has the potential to enhance the coverage of up to 35 dB at 5G mm-wave frequency bands.

Conclusion

In this study, an ultra-compact dual-band FSS design for satellite communication and 5G band coverage augmentation is presented. For the first time, this study has experimentally shown the coverage enhancement for all 5G bands at 24 GHz and 38 GHz, and the Ku band. Compared to the state-of-the-art, the suggested simple single-layered metasurface is compact and polarization insensitive, and it has demonstrated high performance at both bands with oblique incidence angles of up to $60°$. The FSS design constituting 32×32 unit cells with a total size of $96 \times 96\,\text{mm}^2$ has been fabricated and measured. For the transmission coefficient $|S_{21}|$ below -10 dB, the design has attained a fractional bandwidth of 49.5% (14.5–26.4 GHz) and 66.57% (39.8–41.8 GHz) at 24 and 38 GHz bands, respectively. For a reflection coefficient $|S_{11}|$ lower than -10 dB, the design has achieved a transmission band from 29.5 to 31.2 GHz. There is a strong correlation between the simulated and measured results. Due to its overall superior performance, the presented FSS is a viable choice for coverage enhancement in 5G and advanced wireless communication systems. In future, the proposed FSS design can be used to enhance antenna performance in terms of gain and isolation. It can also be employed for beam steering applications. The proposed FSS design can be easily adapted for Reflective Intelligent Surface (RIS) applications due to design symmetry.

Data availability

The datasets used and/or analysed during the current study available from the corresponding author on reasonable request.

References

1. Islam, S., Zada, M. & Yoo, H. Highly compact integrated sub-6 GHz and millimeter-wave band antenna array for 5G smartphone communications. *IEEE Trans. Antennas Propag.* **70**, 11629–11638. https://doi.org/10.1109/TAP.2022.3209310 (2022).
2. Wang, R., Yang, Y., Makki, B. & Shamim, A. A wideband reconfigurable intelligent surface for 5G millimeter-wave applications. *IEEE Trans. Antennas Propag.* **72**, 2399–2410. https://doi.org/10.1109/TAP.2024.3352828 (2024).
3. Hong, T., Guo, S., Jiang, W. & Gong, S. Highly selective frequency selective surface with ultrawideband rejection. *IEEE Trans. Antennas Propag.* **70**, 3459–3468. https://doi.org/10.1109/TAP.2021.3137453 (2022).
4. Liao, W. J. et al. An FSS-integrated low-RCS radome design. *IEEE Antennas Wirel. Propag. Lett.* **18**, 2076–2080. https://doi.org/10.1109/LAWP.2019.2937556 (2019).
5. Ni, Y., Xiong, Q., Zhang, S. W. & Lou, Y. Multi band FSS for 5G signal enhancement. In *2023 IEEE International Students' Conference on Electrical, Electronics and Computer Science, SCEECS 2023* (Institute of Electrical and Electronics Engineers Inc., 2023). https://doi.org/10.1109/SCEECS57921.2023.10062970.
6. Hakim, M. L., Islam, M. T. & Alam, T. Incident angle stable broadband conformal mm-Wave FSS for 5G (n257, n258, n260, and n261) band EMI shielding application. *IEEE Antennas Wirel. Propag. Lett.* **23**, 488–492. https://doi.org/10.1109/LAWP.2023.3326868 (2024).
7. Hakim, M. L., Alam, T. & Islam, M. T. Polarization-insensitive and oblique incident angle stable miniaturized conformal FSS for 28/38 GHz mm-Wave band 5G EMI shielding applications. *IEEE Antennas Wirel. Propag. Lett.* **22**, 2644–2648. https://doi.org/10.1109/LAWP.2023.3284860 (2023).
8. Martinez-De-Rioja, E. et al. Passive intelligent reflecting surfaces based on reflectarray panels to enhance 5G millimeter-wave coverage. *Int. J. Microw. Wirel. Technol.* **15**, 3–14. https://doi.org/10.1017/S1759078722000721 (2023).
9. Tejas, K. S., Udaykumar, M., Varun, R., Suhailkhan & Kumar, T. D. Intelligent reflecting surface assisted wireless communication for coverage enhancement. In *International Conference on Smart Systems for Applications in Electrical Sciences, ICSSES 2023* (Institute of Electrical and Electronics Engineers Inc., 2023). https://doi.org/10.1109/ICSSES58299.2023.10200009.
10. Shah, I. A., Zada, M., Shah, S. A. A., Basir, A. & Yoo, H. Flexible metasurface-coupled efficient wireless power transfer system for implantable devices. *IEEE Trans. Microw. Theory Tech.* **72**, 2534–2547. https://doi.org/10.1109/TMTT.2023.3319050 (2024).
11. Yamamoto, S., Nakazato, J. & Tran, G. K. Multi-IRS-assisted mmWave UAV-BS network for coverage extension. *Sensors* **24**, https://doi.org/10.3390/s24062006 (2024).

12. Mahbub, M. & Shubair, R. M. Coverage enhancement of UAV-enabled 6G networks via intelligent reflecting surfaces: Towards optimal SINR. *Telecommun. Syst.* **83**, 147–157. https://doi.org/10.1007/s11235-023-00999-2 (2023).

13. Hong, T., Wang, M., Peng, K., Zhao, Q. & Gong, S. Compact ultra-wide band frequency selective surface with high selectivity. *IEEE Trans. Antennas Propag.* **68**, 5724–5729. https://doi.org/10.1109/TAP.2020.2963905 (2020).

14. Lin, B. et al. Second-order polarization rotating frequency-selective surface. *IEEE Trans. Antennas Propag.* **69**, 7976–7981. https://doi.org/10.1109/TAP.2021.3076243 (2021).

15. Chiu, C. N. & Chang, K. P. A novel miniaturized-element frequency selective surface having a stable resonance. *IEEE Antennas Wirel. Propag. Lett.* **8**, 1175–1177. https://doi.org/10.1109/LAWP.2009.2034766 (2009).

16. Wu, W., Liu, X., Cui, K., Ma, Y. & Yuan, Y. An ultrathin and polarization-insensitive frequency selective surface at Ka-band. *IEEE Antennas Wirel. Propag. Lett.* **17**, 74–77. https://doi.org/10.1109/LAWP.2017.2774825 (2018).

17. Ramachandran, T., Faruque, M. R. I. & Islam, M. T. Symmetric square shaped metamaterial structure with quintuple resonance frequencies for S, C, X and Ku band applications. *Sci. Rep.* **11**, https://doi.org/10.1038/s41598-021-83715-x (2021).

18. Tariq, S., Rahim, A. A., Sethi, W. T., Faisal, F. & Djerafi, T. Metasurface based antenna array with improved performance for millimeter wave applications. *AEU - Int. J. Electron. Commun.* **177**, https://doi.org/10.1016/j.aeue.2024.155195 (2024).

19. Dai, X. W., Zhang, Y. H., Yu, W., Liu, L. & Luo, G. Q. Dual-wideband dual-circularly polarized reflectarray based on multiresonant structure for K-band and Ka-band applications. *IEEE Antennas Wirel. Propag. Lett.* **23**, 868–872. https://doi.org/10.1109/LAWP.2023.3337504 (2024).

20. Aziz, R. S., Koziel, S., Leifsson, L. & Szczepanski, S. A Study of mutual coupling suppression between two closely spaced planar monopole antenna elements for 5G new radio massive MIMO system applications. *Electronics (Switzerland)* **12**, https://doi.org/10.3390/electronics12122630 (2023).

21. Khan, D., Ahmad, A. & Choi, D. Y. Dual-band 5G MIMO antenna with enhanced coupling reduction using metamaterials. *Sci. Rep.* **14**, https://doi.org/10.1038/s41598-023-50446-0 (2024).

22. Malik, B. T., Khan, S. & Koziel, S. Design and implementation of multi-band reflectarray metasurface for 5G millimeter wave coverage enhancement. *Sci. Rep.* **14**, https://doi.org/10.1038/s41598-024-66330-4 (2024).

Acknowledgements

Author contributions
Conceptualization, B.T.M. (Bilal Tariq Malik) and S.Kh. (Shahid Khan); Data curation, S.K. (Slawomir Koziel) and B.T.M.; Formal analysis, B.T.M.; Funding acquisition, S.K; Visualization, B.T.M. and S.K.; Writing-original draft, B.T.M. and S.Kh.; Writing-review and editing, S.K. and S.Kh.; Sofware and Resources, S.K; Supervision, S.K.

Declarations

Competing interests
The authors declare no competing interests.

Additional information
Correspondence and requests for materials should be addressed to S.K.

Reprints and permissions information is available at www.nature.com/reprints.

Publisher's note Springer Nature remains neutral with regard to jurisdictional claims in published maps and institutional affiliations.